# ORIGINAL ARTICLE

# MicroRNA-138 and MicroRNA-25 Down-regulate Mitochondrial Calcium Uniporter, Causing the Pulmonary Arterial Hypertension Cancer Phenotype

Zhigang Hong[1], Kuang-Hueih Chen[1], Asish DasGupta[1], Francois Potus[2], Kimberly Dunham-Snary[1], Sebastien Bonnet[2], Lian Tian[1], Jennifer Fu[1], Sandra Breuils-Bonnet[2], Steeve Provencher[2], Danchen Wu[1], Jeffrey Mewburn[1], Mark L. Ormiston[1], and Stephen L. Archer[1]

[1]Department of Medicine, Queen's University, Kingston, Ontario, Canada; and [2]Pulmonary Hypertension Research Group of the University Cardiology and Pulmonary Institute of the Quebec Research Centre, Laval University, Quebec City, Quebec, Canada

## Abstract

**Rationale:** Pulmonary arterial hypertension (PAH) is an obstructive vasculopathy characterized by excessive pulmonary artery smooth muscle cell (PASMC) proliferation, migration, and apoptosis resistance. This cancer-like phenotype is promoted by increased cytosolic calcium ($[Ca^{2+}]_{cyto}$), aerobic glycolysis, and mitochondrial fission.

**Objectives:** To determine how changes in mitochondrial calcium uniporter (MCU) complex (MCUC) function influence mitochondrial dynamics and contribute to PAH's cancer-like phenotype.

**Methods:** PASMCs were isolated from patients with PAH and healthy control subjects and assessed for expression of MCUC subunits. Manipulation of the pore-forming subunit, MCU, in PASMCs was achieved through small interfering RNA knockdown or MCU plasmid-mediated up-regulation, as well as through modulation of the upstream microRNAs (miRs) miR-138 and miR-25. *In vivo*, nebulized anti-miRs were administered to rats with monocrotaline-induced PAH.

**Measurements and Main Results:** Impaired MCUC function, resulting from down-regulation of MCU and up-regulation of an inhibitory subunit, mitochondrial calcium uptake protein 1, is central to PAH's pathogenesis. MCUC dysfunction decreases intramitochondrial calcium ($[Ca^{2+}]_{mito}$), inhibiting pyruvate dehydrogenase activity and glucose oxidation, while increasing $[Ca^{2+}]_{cyto}$, promoting proliferation, migration, and fission. In PAH PASMCs, increasing MCU decreases cell migration, proliferation, and apoptosis resistance by lowering $[Ca^{2+}]_{cyto}$, raising $[Ca^{2+}]_{mito}$, and inhibiting fission. In normal PASMCs, MCUC inhibition recapitulates the PAH phenotype. In PAH, elevated miRs (notably miR-138) down-regulate MCU directly and also by decreasing MCU's transcriptional regulator cAMP response element–binding protein 1. Nebulized anti-miRs against miR-25 and miR-138 restore MCU expression, reduce cell proliferation, and regress established PAH in the monocrotaline model.

**Conclusions:** These results highlight miR-mediated MCUC dysfunction as a unifying mechanism in PAH that can be therapeutically targeted.

**Keywords:** mitochondrial calcium uptake protein 1; microRNA-25- and -138-5p; cAMP response element–binding protein; pyruvate dehydrogenase

Pulmonary arterial hypertension (PAH) is an obstructive, arterial vasculopathy in which disorders of endothelial cells, pulmonary artery smooth muscle cells (PASMCs), fibroblasts, and inflammatory cells cause loss of vascular lumen, vascular stiffening, and vasoconstriction (1). This adverse vascular remodeling increases right ventricular (RV) afterload, ultimately causing death from RV failure. Although vasoconstriction is a major pathophysiologic feature in only approximately 5% of patients (2), the approved PAH-targeted therapeutics are primarily vasodilators. Consequently,

## At a Glance Commentary

### Scientific Knowledge on the Subject:
Vascular cells in pulmonary arterial hypertension (PAH) exhibit a cancer-like phenotype, characterized by excessive proliferation and apoptosis resistance. Previous studies have identified multiple abnormalities that may account for this phenotype. However, there has been insufficient focus on finding unifying mechanisms that explain substantial portions of the syndrome.

### What This Study Adds to the Field:
We report that in PAH, decreased function of the mitochondrial calcium uniporter (MCU) complex, caused primarily by down-regulation of its MCU subunit, accounts for much of the cancer-like, mitochondrial-metabolic phenotype in PAH. Increased expression of the microRNAs (miRs) miR-138 and miR-25 down-regulate MCU and cAMP response element–binding protein 1. This underlies much of the ionic, metabolic, and mitochondrial dynamic fingerprint in PAH. Preclinical studies suggest that excess proliferation and apoptosis resistance in PAH can be reversed by augmenting MCU function. We also demonstrate the feasibility of *in vivo* therapy with nebulized anti–miR-138 as a novel PAH therapy.

prognosis remains poor with survival rates of approximately 50% at 5 years (2). This suggests the need to better understand and therapeutically target nonvasospastic pathways, such as PAH's cancer-like phenotype, which is exemplified by excessive proliferation and apoptosis resistance. Underlying this phenotype are cancer-like changes in mitochondrial metabolism (1, 3) and dynamics (4, 5), as well as an increase in intracellular calcium and plasmalemmal membrane depolarization that is secondary to the down-regulation of voltage-gated potassium channels (6).

In PAH PASMCs (7, 8) and endothelial cells (9) glycolysis is uncoupled from glucose oxidation. This metabolic shift, first observed in cancer cells by Warburg (10), results in part

from pyruvate dehydrogenase (PDH) kinases–mediated inhibition of PDH (3), which suppresses apoptosis while increasing proliferation (1, 3). Recently another mitochondrial abnormality has been discovered in PAH PASMCs, namely fragmentation of the mitochondrial network. This is due to increased fission, caused by post-translational activation of dynamin-related protein 1 (Drp1) (4), and impaired fusion, caused by down-regulation of mitofusin-2 (11).

Vasoconstriction and cell proliferation in PAH are also driven by elevation of cytosolic calcium ($[Ca^{2+}]_{cyto}$) (12), resulting from increased calcium influx through the L-type calcium channel (caused by impaired expression of potassium channels, including Kv1.5 [12, 13]), activation of TrpC6 (14) channels, and calcium sensitization (6). Regulation of intracellular calcium and mitochondrial bioenergetics are closely linked. Increases in intramitochondrial $Ca^{2+}$ ($[Ca^{2+}]_{mito}$) accelerate oxidative metabolism by activating mitochondrial dehydrogenases, either directly (oxoglutarate dehydrogenase and isocitrate dehydrogenase) or indirectly (by activating PDH phosphatase, which activates PDH [15–17]). Although it has long been known that mitochondrial calcium stores communicate with cytosolic and sarcoplasmic reticular calcium pools, it is unknown how dysregulation of $[Ca^{2+}]_{cyto}$ and $[Ca^{2+}]_{mito}$ are linked to mitochondrial metabolism and dynamics.

Indeed, the molecular mediators of inflow (18, 19) and egress (20, 21) of mitochondrial calcium have only recently been identified. Calcium enters the mitochondria via the mitochondrial calcium uniporter (MCU) complex (MCUC), an inwardly rectifying, $Ca^{2+}$-selective, ion channel in the inner mitochondrial membrane (22). The MCUC's high $Ca^{2+}$ selectivity at low $[Ca^{2+}]_{cyto}$ (22) allows mitochondrial uptake and release of calcium to dynamically buffer $[Ca^{2+}]_{cyto}$ (23). The MCUC has five components, including the mitochondrial calcium uptake protein 1 (MICU1), an inhibitory calcium-binding protein in the mitochondrial intermembrane space (24), and the pore-forming MCU subunit, a 40-kD protein in the inner mitochondrial membrane (18, 25, 26). Although loss of MCU is not lethal to cells (or mice), it reduces

mitochondrial matrix calcium (18) and lowers PDH activity in skeletal muscle (15). In contrast, MCU overexpression increases mitochondrial matrix calcium (18), which sensitizes cells to apoptotic stimuli (27).

We report that decreased MCUC function, caused by decreased expression of MCU and increased expression of MICU1, underlies key phenotypic features of PAH including elevation of $[Ca^{2+}]_{cyto}$, reduction of $[Ca^{2+}]_{mito}$, mitochondrial fragmentation, and the Warburg phenomenon. Expression of the MCU subunit is post-transcriptionally down-regulated by several microRNAs (miRs), notably hsa-miR-138-5p and hsa-miR-25-3p (henceforth referred to as miR-138 and miR-25). These miRs also inhibit cAMP response element–binding protein 1 (CREB1), which transcriptionally reinforces the down-regulation of MCU. In normal PASMCs, inhibition of the MCUC using ruthenium red or small interfering RNA targeting MCU (si-MCU) recapitulates the PAH phenotype. Conversely, restoring MCU expression in PAH cells, by transfection with the MCU plasmid or anti-miRs, corrects calcium homeostasis, mitochondrial dynamics, and metabolism. *In vivo* anti–miR-25 and anti–miR-138 restore MCU expression and reverse established PAH. These findings establish a central and therapeutically relevant role for the MCUC in PAH.

The results in the current manuscript have not been reported previously in any form.

## Methods

Complete methods can be found in the online supplement.

### Cell Culture
PASMC cultures were established from patients with PAH and control subjects. The identity of PASMCs was confirmed morphologically and by immunohistochemical demonstration of the presence of smooth muscle α-actin and the absence of von Willebrand factor. A primary culture of PASMCs was established and then the cells were harvested with trypsin, frozen in freezing media (10% dimethylsulfoxide, 20% fetal bovine serum, and 70% M231), and stored
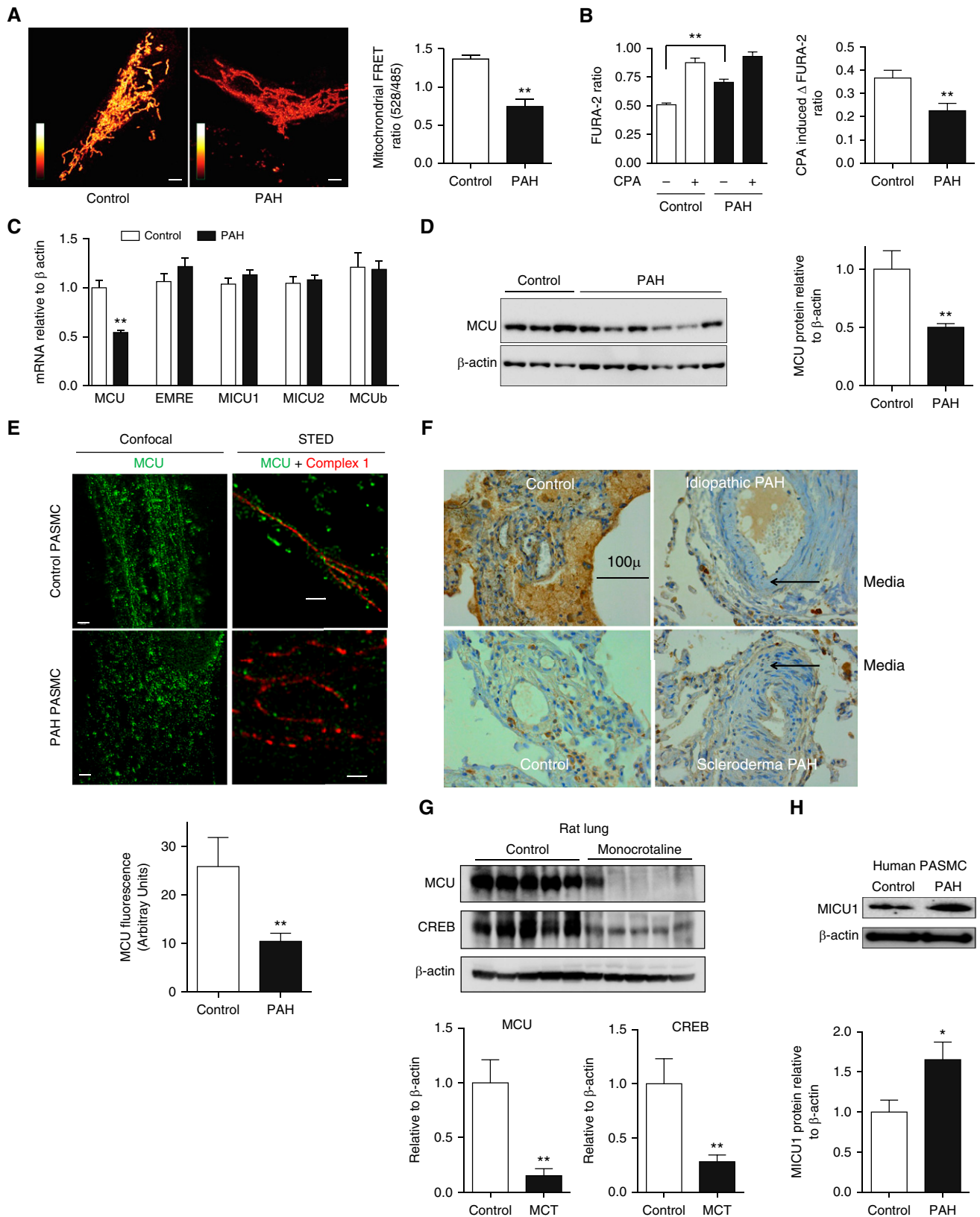
**Figure 1.** Reduced expression of the mitochondrial calcium uniporter (MCU) and decreased intramitochondrial calcium in pulmonary artery smooth muscle cells (PASMCs) in human and experimental pulmonary arterial hypertension (PAH). (*A*) Representative images and mean values for intramitochondrial calcium in control subject and patients with PAH measured using a calcium-sensitive fluorescent Förster resonance energy transfer

in liquid nitrogen for later use. PASMCs were used within the first six passages in culture.

## Statistics

Values are stated as mean ± SEM. When applicable, normality was confirmed with a Kolmogorov-Smirnov test. Intergroup differences were assessed by Student's *t* tests (unpaired or paired) or analysis of variance (simple or repeated-measures), as appropriate. *Post hoc* analysis was performed using Tukey test. A *P* less than 0.05 was considered statistically significant.

## Results

### Low Intramitochondrial Calcium Levels and Reduced MCU Expression in PAH

Assessment of calcium localization using a FURA probe (for $[Ca^{2+}]_{cyto}$) and a Förster resonance energy transfer probe (for $[Ca^{2+}]_{mito}$) demonstrated elevated $[Ca^{2+}]_{cyto}$ and depressed $[Ca^{2+}]_{mito}$ in human PAH PASMCs versus control subjects (Figures 1A and 1B). The cyclopiazonic acid–releasable sarcoplasmic reticulum calcium pool was also reduced in PAH (Figure 1B). To determine which MCUC subunits mediate this shift in calcium compartmentalization, an mRNA expression profile was conducted. This screen revealed an isolated reduction of MCU mRNA in human PAH PASMCs (Figure 1C). Down-regulation of MCU protein was confirmed in human PASMCs (Figures 1D and 1E) and the lungs of patients with PAH (Figure 1F; *see* Figures E1A and E1B in the online supplement).

Super-resolution confocal microscopy showed mitochondrial fragmentation in PAH PASMCs; moreover, the expression of MCU was decreased and its normally well-ordered distribution disrupted (Figure 1E). Similar down-regulation of MCU was evident in lungs of rats with monocrotaline-induced PAH (MCT-PAH) (Figure 1G; *see* Figure E2) and primary cultures of PASMCs derived from resistance level arteries of rats with MCT-PAH or exposure to SU5416 plus chronic hypoxia (*see* Figure E1C). Of note, cAMP response element–binding protein 1, a known regulator of MCU, was also decreased in the lungs of MCT-challenged rats (Figure 1G). Although mRNA levels of other MCUC subunits were unaltered (Figure 1C), a screen of these proteins by Western blotting revealed a significant increase in MICU1 in human PAH PASMCs, and a reduction in MCUb (Figure 1H; *see* Figure E3).

### Decreasing MCU Expression Increases $[Ca^{2+}]_{cyto}$ and Decreases $[Ca^{2+}]_{mito}$

Reduction of MCU with small interfering RNA (siRNA) (*see* Figures E4A and E4B) raised $[Ca^{2+}]_{cyto}$ (Figure 2A) and lowered $[Ca^{2+}]_{mito}$ (Figure 2B), mimicking the PAH calcium phenotype (Figure 2C). $[Ca^{2+}]_{cyto}$ was higher in PAH versus control PASMCs and was reduced in response to the restoration of intramitochondrial MCU expression (Figure 2C) by MCU plasmid transfection (*see* Figures E4D, E5, and E6).

Treatment of PASMCs with the mitochondrial ionophore carbonyl cyanide-4-(trifluoromethoxy)phenylhydrazone (FCCP) was used to establish the size of the

mitochondrial calcium pool. FCCP caused a small but consistent release of mitochondrial calcium into the cytosol in normal PASMCs (Figure 2A) but had no effect in PAH PASMCs (Figure 2C). Transfection of PAH PASMCs with MCU plasmid created a large FCCP-releasable calcium pool (Figure 2C), indicating that restoration of MCU expression replenished the intramitochondrial pool in PAH PASMCs.

### MCUC Inhibition Causes Mitochondrial Fission

As reported previously (4), the mitochondrial network is fragmented in PAH PASMCs (Figures 2D and 2E). To confirm that this fragmentation reflects decreased mitochondrial connectivity we measured the mitochondrial networking factor (MNF), a validated measure of fission (*see* Video 1) (4, 5). In normal human PASMCs, siRNA knockdown of MCU (Figure 2D) or inhibition of MCUC function with ruthenium red fragmented the mitochondrial network and decreased MNF (Figures 2F and 2G), recapitulating the PAH network morphology. Ruthenium red induced mitochondrial fragmentation within 5 minutes (*see* Video 2). In PAH PASMCs, the MNF is significantly reduced versus control (Figures 2E–2G). MCU plasmid transfection of these cells restored mitochondrial network morphology and increased MNF.

### Inhibition of MCU Mediates the Warburg Effect in PAH PASMCs

We used micropolarimetry to measure mitochondrial respiration in cultured PASMCs (8). When compared with PAH PASMCs, control PASMCs had a

**Figure 1.** (*Continued*). (FRET) probe (a cyan fluorescent protein–calmodulin–yellow fluorescent protein construct) by confocal microscopy (n = 10; \*\**P* < 0.01). The FRET ratio (528/485 nm) depends on the probe's calmodulin conformation, which is determined by the amount of bound calcium and shown with *white* reflecting higher intramitochondrial calcium concentration than *red*, as described (56). *Ratio bar* is from 0 to 2.5, *scale bar* = 5 μm. (*B*) Cytosolic calcium, measured using FURA-2, is increased in PAH PASMCs (n = 25; \*\**P* < 0.01). The amount of calcium within the sarcoplasmic reticulum (the pool released by cyclopiazonic acid [CPA]) is reduced in PAH versus control PASMCs (n = 25; \*\**P* < 0.01). (*C*) Quantitative reverse-transcription polymerase chain reaction measurement of mRNA expression for each of the MCU complex's components. Only the expression of MCU mRNA is altered in human PAH PASMCs (n = 6–7; \*\**P* < 0.01). (*D*) Representative immunoblots and densitometric quantification demonstrating decreased MCU protein expression in human PAH versus control PASMCs (n = 4–7; \*\**P* < 0.01). (*E*) Confocal (*left*) and stimulated emission depletion (STED) super-resolution (*right*) images of the mitochondrial network of control (*top*) and PAH (*bottom*) human PASMCs. In normal patients, STED images reveal that MCU (*green*) is localized in uniform discrete bands spanning the inner mitochondrial membrane into the matrix, where NADH dehydrogenase (complex I, *red*) is located. *Scale bar* = 2 μm for confocal images and 0.5 μm for STED images. (*F*) Representative immunohistochemistry of human control versus PAH lungs (of n = 10 per group) demonstrating increased expression of MCU protein (*brown*) in the media and endothelium of pulmonary arteries (representative of >10 patients/group; *see* additional images in Figures E1A and E1B). The increased medial thickness (*arrows*) is visible in the small pulmonary arteries of patients with PAH. *Scale bar* = 100 μm. Representative immunoblots and densitometric quantification showing (*G*) decreased expression of MCU and its transcriptional regular cAMP response element–binding protein 1 (CREB1) in lungs from rats with monocrotaline (MCT)-PAH versus control rats (n = 5/group; \*\**P* < 0.01) and (*H*) increased expression of mitochondrial calcium uptake protein 1 (MICU1), a negative regulator of MCU, in human PAH PASMCs (n = 5–7; \**P* < 0.05). EMRE = essential MCU regulator.
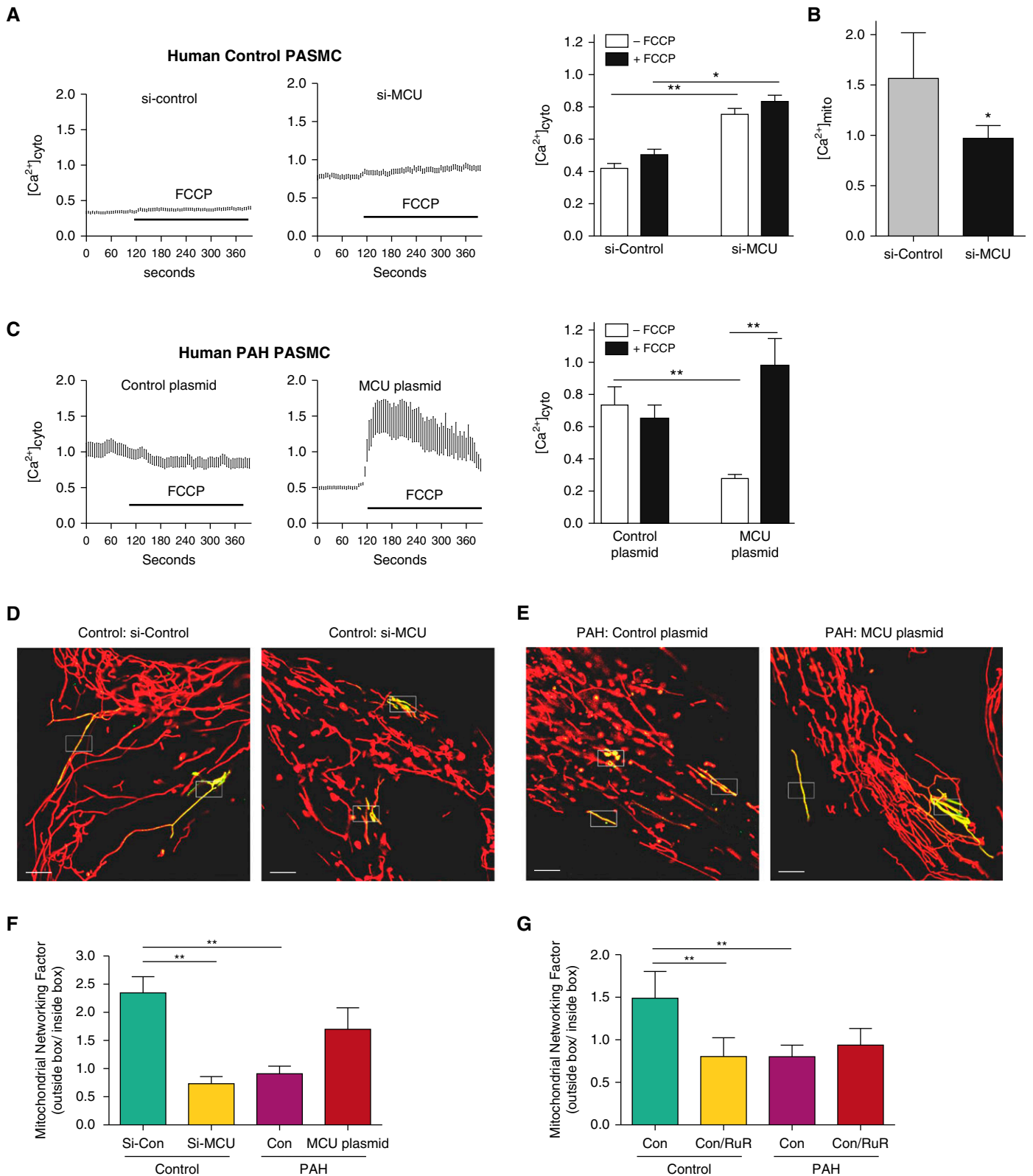
**Figure 2.** Decreased mitochondrial calcium uniporter (MCU) expression in pulmonary arterial hypertension (PAH) causes a reciprocal increase in cytosolic calcium concentration and mitochondrial fission. Cytosolic calcium was measured in human pulmonary artery smooth muscle cells (PASMCs) using fluo-3 and FURA Red (3 μM for 30 min) and expressed as the ratio of 530/640 nm emission measured at 488 nm. (A) Representative and mean data showing cytosolic calcium concentrations are elevated in normal PASMCs when MCU expression is reduced by exposure to small interfering RNA

greater oxygen consumption rate (OCR), and a lower extracellular acidification rate (ECAR, a measure of glycolysis) (Figure 3A). The glycolysis stress test (Figure 3B) demonstrated that both control and PAH PASMCs exhibit similar responses to glucose stimulation and inhibition. Control PASMCs also exhibited a higher ratio of OCR to ECAR (Figure 3C). In addition, the respiratory reserve capacity (the increase in OCR elicited by FCCP) was significantly reduced in PAH PASMCs (Figure 3A). To determine whether changes in MCU expression were sufficient to cause these metabolic changes, we administered si-MCU to normal PASMCs. si-MCU reduced the OCR, increased ECAR, did not change response to glucose stimulation/inhibition, and significantly decreased the OCR/ECAR ratio, recapitulating the Warburg effect seen in PAH PASMCs (Figures 3D–3F). Conversely, transfection of PAH PASMCs with the MCU plasmid reversed the PAH phenotype, reducing uncoupled glycolysis and increasing the OCR/ECAR ratio (Figures 3G–3I).

The basis for reduced OCR in PAH PASMCs is PDH inhibition (Figure 3J). Moreover, molecular or chemical inhibition of MCU inhibited PDH activity in normal PASMCs. This inhibition was exacerbated in PAH PASMCs. si-MCU also increased extracellular lactate production in normal PASMCs (Figure 3K). Conversely, MCU overexpression reduces the elevated lactate production seen in PAH PASMCs. Thus, changes in MCU subunit expression are
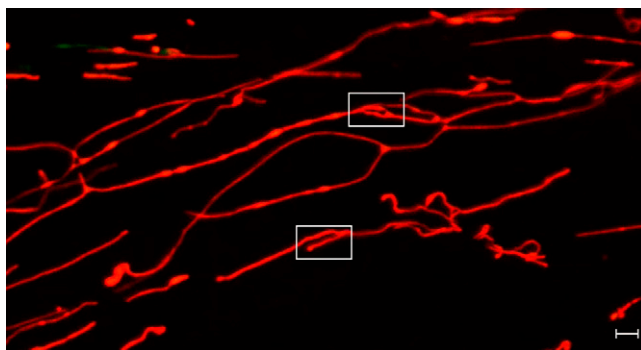


**Video 1.** Mitochondrial networking is measured using a mitochondria-targeted, photoactivatable green fluorescent protein (mito-PA-GFP). Mitochondrial networking was evaluated by transfecting pulmonary artery smooth muscle cells with a Mito-PA-GFP plasmid (FuGENE HD Transfection Reagent, 1 ng/2 ml, 72 h). Cells were also incubated with tetramethylrhodamine (10 nM, 37°C, 30 min incubation), a potentiometric dye, which is taken up by mitochondria in proportion to the negativity of their membrane potential (*red*). PA-GFP was photoactivated in a defined area (*rectangular boxes*). We then calculated the mitochondrial networking factor, as previously described. In brief, the number of green pixels outside the activation box was measured at the first image (5 s) after photoactivation and divided by the number of green pixels (activated PA-GFP) inside the boxed activation area. *Scale bar* = 1 $\mu$m. The movie duration is 2 minutes. The mitochondrial network was imaged with a Leica STED super-resolution confocal microscope (Leica, Wetzlar, Germany) at ×63 magnification and ×4 digital zoom.
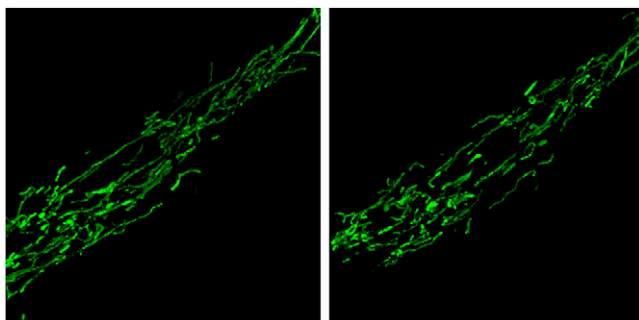


**Video 2.** The mitochondrial calcium uniporter complex inhibitor ruthenium red causes mitochondrial fission. The mitochondrial network was imaged with a Leica STED super-resolution confocal microscope (Leica, Wetzlar, Germany) at ×100 magnification and ×4 digital zoom. Cells were loaded with MitoTracker Green (100 nM for 20 min at 37°C; ThermoFisher Scientific, Waltham, MA) and imaged both (*A*) before and (*B*) after ruthenium red at excitation/emission wavelengths of 488 and 530 nm, respectively. The total image size is 38.7 $\mu$m$^2$. The duration of both movies is 5 minutes.

**Figure 2.** (Continued). targeting MCU (si-MCU) (10 nM for 72 h), partially recapitulating the PAH phenotype (n = 3 individual cell lines per group, with a total of 6–17 cell images per line; *$P < 0.05$, **$P < 0.01$). (*B*) si-MCU reduces intramitochondrial calcium, demonstrating the role MCU expression plays in establishing a reciprocal relationship between mitochondrial and cytosolic calcium concentration (n = 3 control human PASMC lines, six discrete cell measurements per line; *$P < 0.05$). (*C*) Cytosolic calcium is higher in PAH versus control PASMCs. Overexpressing MCU by plasmid transfection (1 ng DNA/2 ml for 72 h) lowered the baseline cytosolic calcium level in PAH PASMCs to near normal control levels (*A*). In addition, MCU transfection greatly augmented the intramitochondrial calcium pool (which is reflected by the significantly greater increase in cytosolic calcium), which occurs in response to the mitochondrial uncoupling agent, carbonyl cyanide-4-(trifluoromethoxy)phenylhydrazone (FCCP) (1 $\mu$M) (n = 3 individual cell lines per group, with a total of 6–17 cell images per line; *$P < 0.05$, **$P < 0.01$). (*D–G*) PASMCs were transfected with photoactivatable, mitochondrial-targeted green fluorescent protein (Mito-PA-GFP) and then loaded with a potentiometric dye, tetramethylrhodamine (10 nM at 37°C for 30 min). Mitochondrial networking was evaluated with photoactivating Mito-PA-GFP as described in the METHODS section in the online supplement. Mitochondrial networking factor (MNF), a metric that is proportionate to the degree of fusion, is calculated as the number of green pixels outside the *white photoactivation boxes* measured in the first image after photoactivation (5 s) divided by the number of green pixels within the activation area, as previously described (4, 5). *Scale bar* = 5 $\mu$m. Representative images (*D* and *E*) and mean ± SEM data (*F*) show a fused mitochondrial network (high MNF) in normal human PASMCs versus a fragmented network in identically imaged PAH PASMCs (low MNF). Inhibiting MCU expression in normal PASMCs (using si-MCU) recapitulates the PAH phenotype. Conversely, MCU overexpression in PAH PASMCs (using MCU plasmid transfection) restores the network fusion (n = 3 individuals per group, with experiments on each individual cell line repeated five to seven times; *$P < 0.05$; **$P < 0.01$). (*G*) The MCUC inhibitor ruthenium red (RuR; 10 $\mu$M for 48 h) mimics the effects of si-MCU, leading to fragmentation (reduced MNF). RuR had no additional effects on the already fragmented mitochondrial network of PAH PASMCs (n = 3 individuals per group, with experiments on each individual cell line repeated three to five times; **$P < 0.01$). [Ca$^{2+}$]$_{cyto}$ = cytosolic calcium concentration; [Ca$^{2+}$]$_{mito}$ = intramitochondrial calcium concentration; Con = control; si-control = scrambled siRNA control.
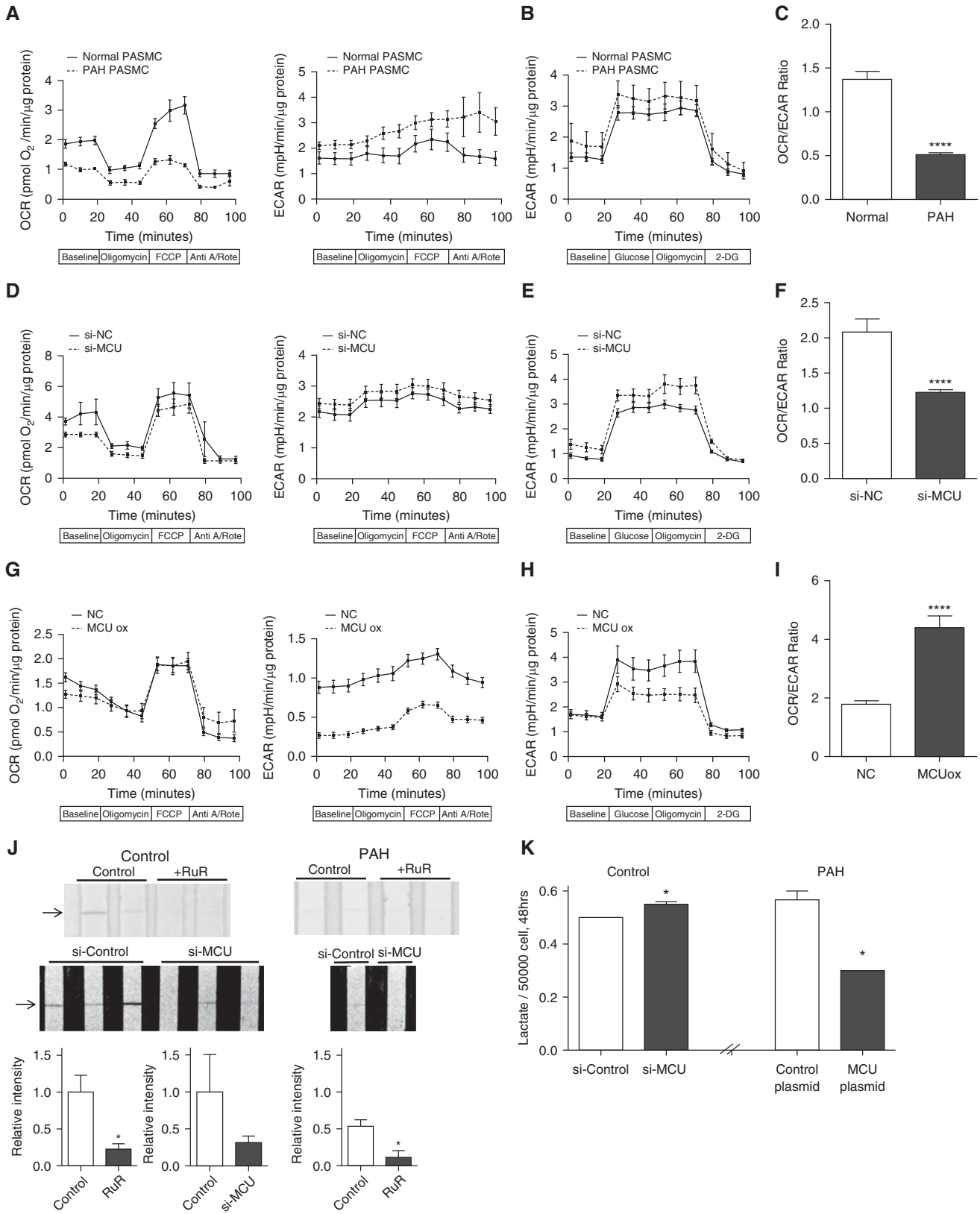
**Figure 3.** Mitochondrial calcium uniporter (MCU) gene transfer restores pyruvate dehydrogenase (PDH) activity and improves the coupling of glycolysis to glucose oxidation in pulmonary arterial hypertension (PAH) pulmonary artery smooth muscle cells (PASMCs). (*A–I*) Oxygen consumption rate (OCR) and extracellular acidification rate (ECAR) as markers of mitochondrial and glycolytic flux were measured in PASMCs using the Seahorse XF®24 Extracellular

sufficient to explain many aspects of the PAH metabolic phenotype.

## Manipulation of MCUC Inhibition Modulates PASMC Migration, Proliferation, and Apoptosis

We assessed whether modulating MCU expression could alter PASMC function, as measured by migration and proliferation (Figure 4). PASMC migration was stimulated using platelet-derived growth factor (PDGF), a mitogen that is up-regulated in PAH, and measured using a modified Boyden chamber and the Xcelligence analyzer (Acea Biosciences Inc., San Diego, CA). Inhibiting MCUC using ruthenium red enhanced migration of both control and PAH PASMCs (Figures 4A and 4B). Although there was no additive effect of combining PDGF and ruthenium red in normal PASMCs, inhibiting the MCUC further increased the rate of migration in PAH PASMCs (Figures 4A and 4B).

Proliferation rates were higher in PAH than control PASMCs (Figure 4C). Chemical or molecular inhibition of the MCUC increased proliferation in normal and PAH PASMCs (Figures 4C and 4D). Conversely, MCU transfection reduced cell proliferation in control and PAH PASMCs (Figure 4E). Knockdown of MICU1 with siRNA (see Figures E4C and E4D) also reduced PASMC proliferation rates in PAH PASMCs but had no effect on control PASMCs (Figure 4F), consistent with the interpretation that some of the enhanced cell proliferation in PAH reflects inhibition of MCUC by MICU1, MCU's negative regulator (Figure 1H). Restoring MCU expression also increases basal apoptosis rates in PAH PASMCs (Figure 4G).

## miR-138 and miR-25 Mediate Post-transcriptional Down-regulation of MCU

We next assessed the molecular basis for depressed MCU expression in PAH. MCU is regulated at the transcriptional level by CREB1 (28), and at the post-transcriptional level by one or more miR (29). In addition to previous reports demonstrating that miR-25 down-regulates MCU expression in cancer cells (29) and cardiomyocytes (30), in silico analysis using Target Scan 7.0 (http://www.targetscan.org/vert_70/) and miRDB (http://mirdb.org/miRDB/index.html) identified miR-138, miR-124, and miR-129 as potentially targeting MCU. Assessment of miR expression by quantitative reverse-transcription polymerase chain reaction identified a significant elevation in miR-138 and a trend toward increased miR-25 in PAH PASMCs (Figure 5A). No differences were observed in the expression of other miRs (data not shown).

In addition, we compared miR expression in PASMCs from six patients with PAH and three healthy subjects using the Affymetrix miRNA 4.0 Microarray (Affymetrix, Santa Clara, CA). Using a prespecified difference threshold of $1.5\times$, we identified six up-regulated miRs in PAH ($P < 0.05$) (see Table E1). None of these species have previously been reported to target MCU and none were identified by our in silico analysis as prospective MCU targets. Therefore, these miR species were not further pursued in this initial study.

In silico target prediction using nucleotide BLAST shows that miR-138 has three predicted target sites within the 3'-UTR of MCU, one of which has an Expect value of 0.36, suggesting a very high likelihood of interaction (see Figures E7A

and E7B). In addition, miR-25 has two predicted sites of interaction with MCU's 3'-UTR (Expect values 1.3 each) (see Figures E7A and E7C). Binding of miR-25 and miR-138 to the 3'-UTR of MCU was directly confirmed in vitro using a luciferase reporter fused to the 3'-UTR of the MCU gene. Cotransfection of HEK293A cells with either miR-25 or miR-138 and the reporter construct resulted in decreased luciferase production, confirming binding of these miRs to the 3'-UTR of MCU (Figure 5B).

These same miRs also regulate CREB1 expression. miR-138 has a predicted target site within CREB1's 3'-UTR (Expect value 1.1). Likewise, miR-25 has three predicted target sites (Expect value 1.1 for each) (see Figures E7D–E7F). To more directly determine the relationship between miR-138 and CREB1 we administered anti–miR-138 and anti–miR-25 to PAH PASMCs and observed that both increased expression of MCU and CREB1 (Figures 5C and 5D), although the therapeutic efficacy varied among individual patients (see Figures E8A and E8B). Thus, the miRs are regulating both MCU and CREB1. Importantly, these beneficial changes were observed in the absence of any significant effect of anti-miRs on miR-25 or miR-138 expression levels (see Figures E8C and E8D). This finding is in keeping with the fact that anti-miRs do not function by reducing miR levels but instead act by preventing the binding of these miRs to the 3'-UTR of target genes.

Because CREB1 is potentially both a target for and a regulator of miRs (31) we inhibited CREB1 in normal PASMCs using a validated si-CREB1 (Figure 5E). The absence of elevated miR expression despite successful down-regulation of CREB1 indicates that miRs are the upstream regulators of the MCU pathway (Figures 5E and 5F).

Figure 3. (Continued). Flux Analyzer (Seahorse XFe24, Agilent Technologies Canada Inc., Mississauga, ON, Canada), as previously described (8). All measurements were made on n = 25,000–50,000 cells/well and five wells per cell line (sample). Each experimental group consisted of two to three patient cell lines (samples). All data were normalized to total protein per well before analysis. (A) OCR (left) is higher and ECAR (right) is lower in naive normal PASMCs compared with PAH PASMCs. (B) Glycolytic activity is higher in naive PAH PASMCs compared with normal. (C) Naive normal PASMCs have a higher OCR/ECAR ratio than PAH PASMCs (****$P < 0.0001$). (D) Silencing MCU using small interfering RNA targeting MCU (si-MCU) reduced OCR (left) and increased ECAR (right) in normal PASMCs. (E) Silencing MCU increased glycolytic activity in normal PASMCs. (F) si-MCU decreases the OCR/ECAR ratio in normal PASMCs (****$P < 0.0001$). (G) OCR is markedly reduced in PAH PASMCs with and without MCU overexpression (MCU ox) (vs. control PASMCs; note smaller scale compared with A and D). Overexpression of MCU (via transfection of MCU plasmid) has little effect on OCR (left) but disproportionately lowers ECAR (right). (H) Glycolytic activity is decreased in PAH PASMCs with MCU overexpression compared with control PAH. (I) MCU overexpression increases the OCR/ECAR ratio in PAH PASMCs (****$P < 0.0001$). (J) Representative images and mean data (n = 4/group; *$P < 0.05$) showing that PDH activity is greater in control PASMCs than in PAH PASMCs and that in both cell types PDH activity is inhibited by the MCU complex inhibitor ruthenium red (RuR; 10 μM) or Si-MCU. PDH activity was measured in homogenized PASMCs using a PDH activity dipstick in which the intensity of the nitroblue tetrazolium band (arrows) is proportionate to enzyme activity (ab109882; MitoSciences-Abcam, Eugene, OR). (K) Lactate production is increased in normal PASMCs by inhibiting MCU expression (using si-MCU) and is reduced in PAH PASMCs by overexpressing MCU (by plasmid transfection) (n = 4; *$P < 0.05$). Data in panels A, B, C, D, and H are mean ± SEM. 2-DG = 2-deoxyglucose; Anti A/Rote = antimycin A and rotenone; FCCP = carbonyl cyanide-4-(trifluoromethoxy)phenylhydrazone; NC = negative control small interfering RNA.
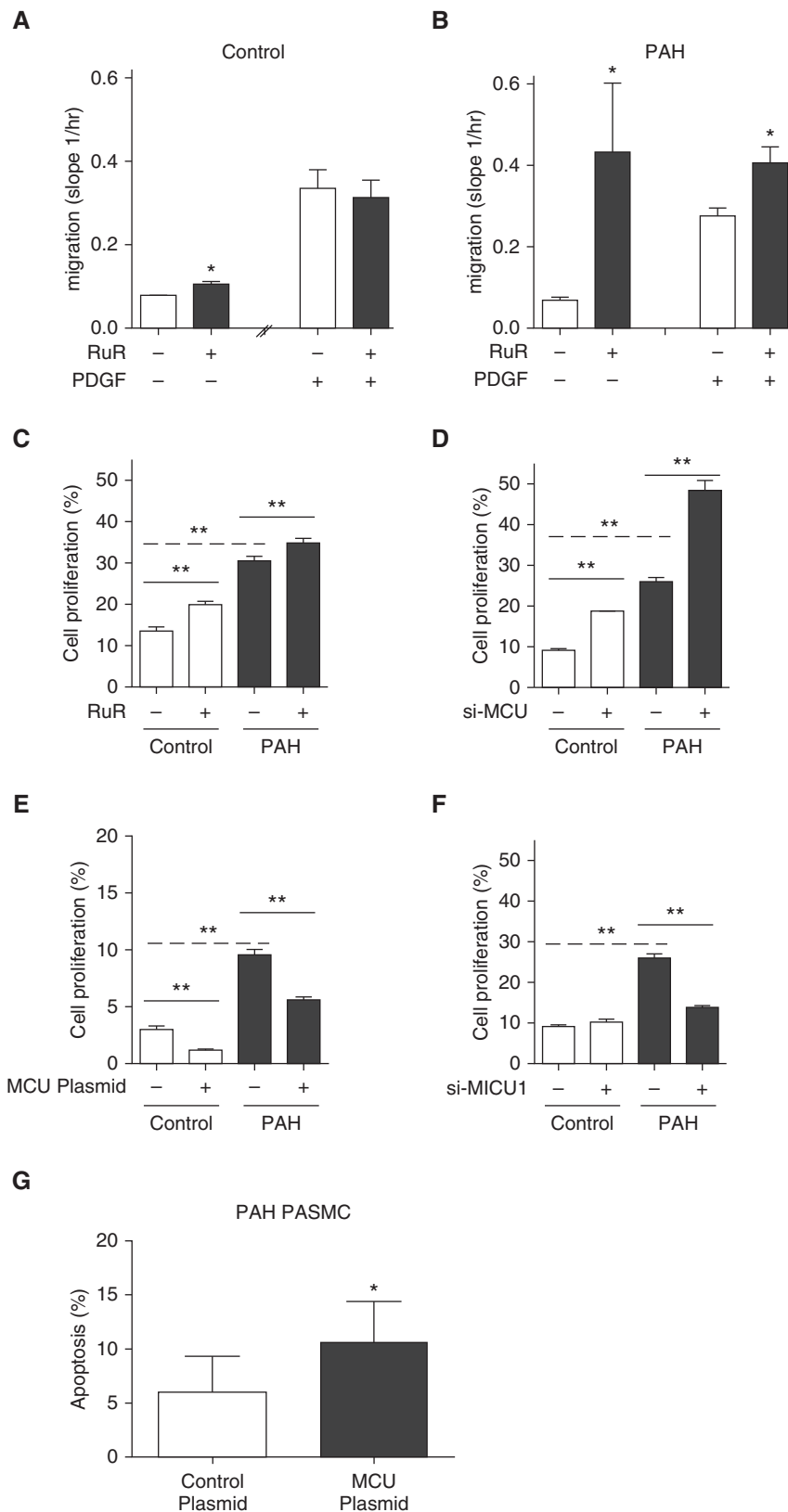
However, both miRs target CREB1's 3′-UTR and the resulting CREB1 down-regulation would be expected to reinforce MCU down-regulation. Supporting this interpretation, si-CREB1 reduces MCU expression in normal human PASMCs (Figure 5F). This is highly relevant because CREB1 expression is reduced in human PAH PASMCs (Figures 5G and 5H) and in lung homogenates of rats with MCT-PAH (Figure 1G). Moreover, serine-133 phospho-CREB1, the transcription factor's activated form (32), is down-regulated in PAH (Figure 5G). To assess CREB1 activity we measured the incidence and intensity of nuclear CREB1 expression using immunofluorescence. CREB1 activity was reduced in PAH and fewer PAH PASMCs had detectable nuclear CREB1 (Figure 5H).

## Inhibition of miR-138 and miR-25 Reverses the MCT Rat Model of PAH

To assess the biologic impact of miR-25 and miR-138 up-regulation on the pathogenesis of PAH, rats with mild established MCT-induced PAH were nebulized with the anti-miRs (anti–miR-138, anti–miR-25, or anti–miR-control) (Figure 6A). Nebulization of anti–miR-25 or anti–miR-138 significantly attenuated disease progression in the MCT model (Figures 6B–6D). The improvements were comprehensive and included reduction in total pulmonary vascular resistance, the result of a large reduction in mean pulmonary artery pressure, and marked increase in cardiac output and RV function, accompanied by a reduction in RV end diastolic pressure and right ventricular hypertrophy. In addition, functional capacity improved dramatically with both anti-miRs (Figure 6B; see Figure E9). Consistent with the finding that miR-138 was the most elevated MCU-targeting species in PAH PASMCs, inhaled anti–miR-138 was more effective in increasing stroke volume than anti–miR-25 (Figure 6B; see Figure E9). Both anti–miR-138 and anti–miR-25 lowered plasma levels of brain natriuretic peptide to control levels, consistent with a reduction in RV pressure/volume overload (see Figure E10). These hemodynamic benefits were accompanied by regression of vascular obstruction, as quantified by a decrease in medial thickness in small pulmonary arteries (Figures 6C and 6D), and a restoration of MCU expression in the pulmonary arteries of MCT-challenged rats (Figure 6E). Dual staining of lung

**Figure 4.** Pulmonary artery smooth muscle cell (PASMC) migration, proliferation, and apoptosis are regulated by the mitochondrial calcium uniporter (MCU). (*A* and *B*) PASMC migration (basal or stimulated by platelet-derived growth factor [PDGF]) was measured using the iCELLigence system, an

sections for MCU and either smooth muscle cell α-actin (Figure 6E) or endothelial CD31 (see Figure E11) suggest that the beneficial effects of anti-miR treatment were likely caused by a restoration of MCU in the vascular smooth muscle cell layer. However, we cannot exclude an additional direct benefit on the pulmonary endothelium or the RV, because MCU down-regulation also occurred in the RV of rats with MCT-PAH (see Figure E12).

## Discussion

Impaired MCUC function is central to the mechanism of human and experimental PAH. MCUC dysfunction is caused by decreased expression of MCU subunit, exacerbated by up-regulation of MICU1, an inhibitory complex subunit. Decreased MCU expression is initiated by an increase in several miRs, notably miR-138 and miR-25. miR-induced MCU down-regulation is reinforced by miR-induced down-regulation of MCU's transcriptional regulator, CREB1. This miR-CREB1-MCUC pathway is schematically illustrated in Figure 6E.

In normal vascular myocytes the mitochondrion's buffering capacity attenuates increases in $[Ca^{2+}]_{cyto}$ caused by increased influx of extracellular calcium or calcium released from the sarcoplasmic reticulum. By attenuating the magnitude and duration of elevations in $[Ca^{2+}]_{cyto}$, mitochondria limit vasoconstriction, cell migration, proliferation, and mitochondrial fission. Additionally, mitochondrial calcium influx through the MCU activates calcium-sensitive dehydrogenases, such as PDH. The reduction in $[Ca^{2+}]_{mito}$, which has previously been noted in PAH (Figure 1) (33), inhibits calcium-sensitive dehydrogenases in the mitochondrial matrix (Figure 3J). When PDH activity is reduced oxidative metabolism declines,

forcing a bioenergetic reliance on aerobic glycolysis, a metabolic switch referred to as the Warburg phenomenon (Figure 3) (10).

Several lines of evidence indicate that impaired MCUC function is critical to disease pathogenesis. For example, in normal human PASMCs, inhibiting the MCUC replicates the PAH phenotype, whether achieved using ruthenium red or si-MCU. In these normal PASMCs, MCU inhibition is sufficient to increase mitochondrial fission and reduce glucose oxidation, increasing cell proliferation and migration (Figure 4). Conversely, in PAH PASMCs, restoring MCU expression by MCU gene transfer lowers $[Ca^{2+}]_{cyto}$ and repletes $[Ca^{2+}]_{mito}$ (Figure 2). Moreover, MCU gene transfer in PAH PASMCs reduces the rate of cell proliferation and migration while increasing both oxidative glucose metabolism and apoptosis (Figures 3 and 4).

Although there are many causes of abnormal metabolism in PAH, including PDH kinases–mediated PDH inhibition (3), it is clear that MCU function, through its ability to regulate $[Ca^{2+}]_{mito}$, has a major effect on PDH activity. In normal PASMCs, si-MCU inhibits PDH and recapitulates the Warburg phenomenon (Figure 3). These metabolic effects of si-MCU are mimicked by ruthenium red (Figure 3). Conversely, augmenting MCU expression in PAH PASMCs reverses the Warburg phenotype, restoring oxidative glucose metabolism, suggesting a potential therapeutic strategy (Figure 3).

PAH PASMCs have a second prominent mitochondrial abnormality, namely mitochondrial fragmentation caused by increased fission (4) and impaired fusion (11) (Figure 2) (34). In PAH and cancer, increased mitotic fission is mediated in part by phosphorylation of Drp1 at serine-616. Increased fission permits rapid cell division, and is coordinated with mitosis via shared dependence on cyclin B-CDK1 (34). Numerous additional Drp1-activating

stimuli exist in the PAH milieu, including increased $[Ca^{2+}]_{cyto}$ (Figure 2), which activates calmodulin kinase, which in turn phosphorylates and activates Drp1 (35). We demonstrate that in normal PASMCs, reducing MCU expression or inhibiting MCUC function increases mitochondrial fission (Figure 2). Conversely, restoring MCU expression in PAH PASMCs is sufficient to fuse the PAH mitochondrial network (Figures 2D–2G).

miRNA dysregulation in the RV, skeletal muscle, and pulmonary vasculature contributes to the progression of PAH (36–39). The following miRs are up-regulated in PAH PASMCs and endothelial cells: miR-130/301, miR-145, miR-21, miR-190, miR-29b, miR-17/92, miR-125, and miR-210 (36, 40). These miRs regulate the following pathways that are relevant to PAH pathophysiology: PPARγ (41), BMPR-II (42, 43), KLF4–5 (44), voltage-gated potassium channels (45), and STAT3 (46). However, this is the first report of the role of miR-138 in either MCU regulation or the development of PAH (Figure 5A). Although miR-138 up-regulation was previously noted in human PAH, its functional importance was not explored (47). Hypoxia-induced increases in miR-138 promote apoptosis resistance and worsen hypoxic pulmonary hypertension by targeting the proapoptotic serine/threonine kinase, MST1, thereby preventing caspase activation and disrupting Bcl-2 signaling (40). Consistent with this report, we observed that MCU down-regulation promoted apoptosis resistance, which was reversed by restoring MCU expression (Figure 4G). Our findings are also consistent with the apoptosis resistance that occurs in cancer due to MCU down-regulation (29, 48).

miR-138 also causes endothelial dysfunction and impairs tube formation by diminishing vascular endothelial growth factor–induced nitric oxide production through a mechanism involving S100A1 (49).

---

**Figure 4.** (Continued). impedance-based system of measuring cell number and cell movement (ACEA Biosciences, San Diego, CA) wherein higher slope indicates faster migration. Ruthenium red (RuR; 10 μM for 6 h) increased PASMC migration in control (A) and pulmonary arterial hypertension (PAH) (B) PASMCs. The increase was additive to that achieved with PDGF in PAH PASMCs (*$P < 0.05$; n = 3/group). (C and D) Rates of PASMC proliferation are faster in PAH versus control PASMCs. RuR (10 μM for 37–41 h) and small interfering RNA targeting MCU (si-MCU) increase rates of cell proliferation in both control and PAH PASMCs (**$P < 0.01$; n = 5/group). Proliferation was measured using a Click-iTEdU kit (Invitrogen, Waltham, MA) according to the manufacturer's instructions. (E) Transfection with the MCU plasmid reduces rates of cell proliferation in both control and PAH PASMCs. Values are mean ± SEM; **$P < 0.01$; n = 5/group. (F) Inhibition of the negative regulator of the mitochondrial calcium uniporter complex, mitochondrial calcium uptake protein 1 (MICU1), using si-MICU1, reduces cell proliferation in PAH PASMCs (**$P < 0.01$; n = 4/group). (G) Transfection with the MCU plasmid increases baseline apoptosis in PAH PASMCs cultured in serum (*$P < 0.05$; n = 4/group).
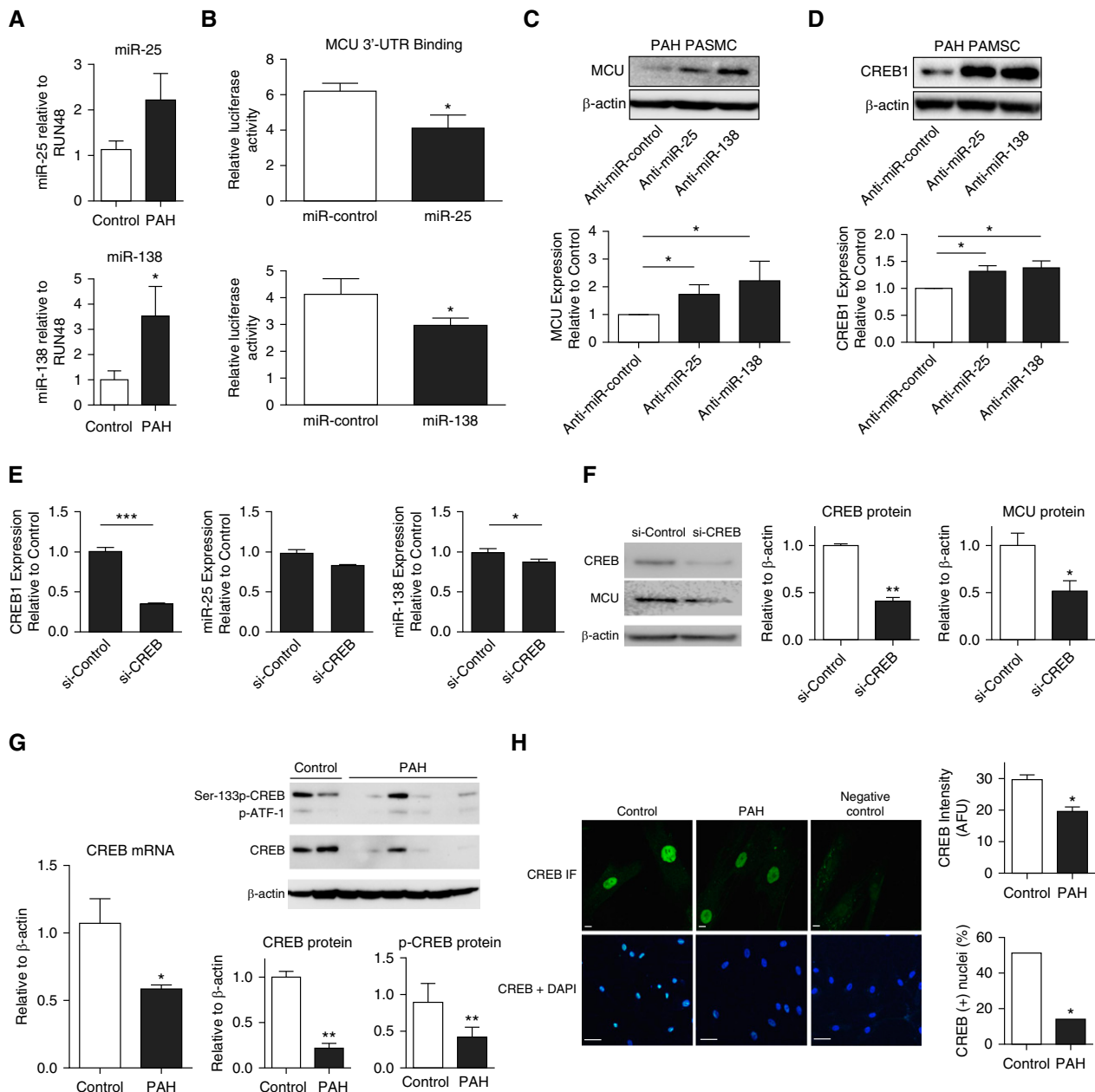
**Figure 5.** Down-regulation of mitochondrial calcium uniporter (MCU) results from increased expression of microRNA (miR)-138 but is reinforced by miR-25 and reduced expression of cAMP response element–binding protein 1 (CREB1). The nomenclature of miRs is in evolution, and because the sequence of rat and human miRs is the same, we use the more generic names, miR-138 and miR-25. However, all anti-miRs were constructed against the human miR sequences for hsa-miR-138-5p and hsa-miR-25-3p. (*A*) Expression of miR-138 is increased in pulmonary arterial hypertension (PAH) pulmonary artery smooth muscle cells (PASMCs) (*$P < 0.01$; $n = 9-12$/group). Note the trend for increased expression of miR-25 ($P =$ NS). (*B*) HEK293A cells were transfected with a luciferase reporter bearing the 3′-UTR of the MCU gene, as well as a miR control, (*A*) miR-25 or (*B*) miR-138. Both miR-25 and miR-138 were found to repress the activity of luciferase reporter, indicating their binding to their target sites in the MCU 3′-UTR (*$P < 0.05$; $n = 6$). (*C* and *D*) Anti–miR-138 and anti–miR-25 restore expression of (*C*) MCU and (*D*) CREB1 mRNA (*top*) and protein (*bottom*) (*$P < 0.01$; $n = 3$/group). (*E*) CREB small interfering RNA (si-CREB) does not significantly increase expression of miR-25 or miR-138 (*$P < 0.05$; ***$P < 0.001$; $n = 3$/group). (*F*) si-CREB1 transfection reduces the expression of CREB1 in normal PASMCs (immunoblot and aggregate data) (*$P < 0.05$; **$P < 0.01$; $n = 4$/group). This leads to a reduction in the expression of MCU protein, thereby confirming the relevance of the observed down-regulation of CREB1 in PAH to the associated reduction in MCU expression in PAH (Figure 6B). (*G*) Quantitative reverse-transcription polymerase chain reaction (*top*) and immunoblot and aggregate data showing that CREB1 and phospho-CREB1 (serine-133; Ser-133p-CREB) expression are decreased in PAH versus control PASMCs (*$P < 0.05$; **$P < 0.01$; $n = 4-6$/group). (*H*) Representative images and mean data showing that expression of activated CREB1, defined as CREB IF (*green*) in the PASMC nucleus, is increased in PAH (*middle column*). *Scale bars* = 10 μm (*top*) and 50 μm (*bottom*). CREB1 intensity is expressed in arbitrary fluorescent units (AFU). In addition, a higher percentage of PAH PASMCs versus control PASMCs have detectable CREB1 immunofluorescence in the nucleus (colocalized with 4′,6-diamidino-2-phenylindole [DAPI]) (*$P < 0.05$; $n = 3$ lines per group; discrete three to four measurements per line). The negative control had no primary antibody. p-ATF-1 = activating transcription factor-1; si-control = scrambled siRNA control; UTR = untranslated region.
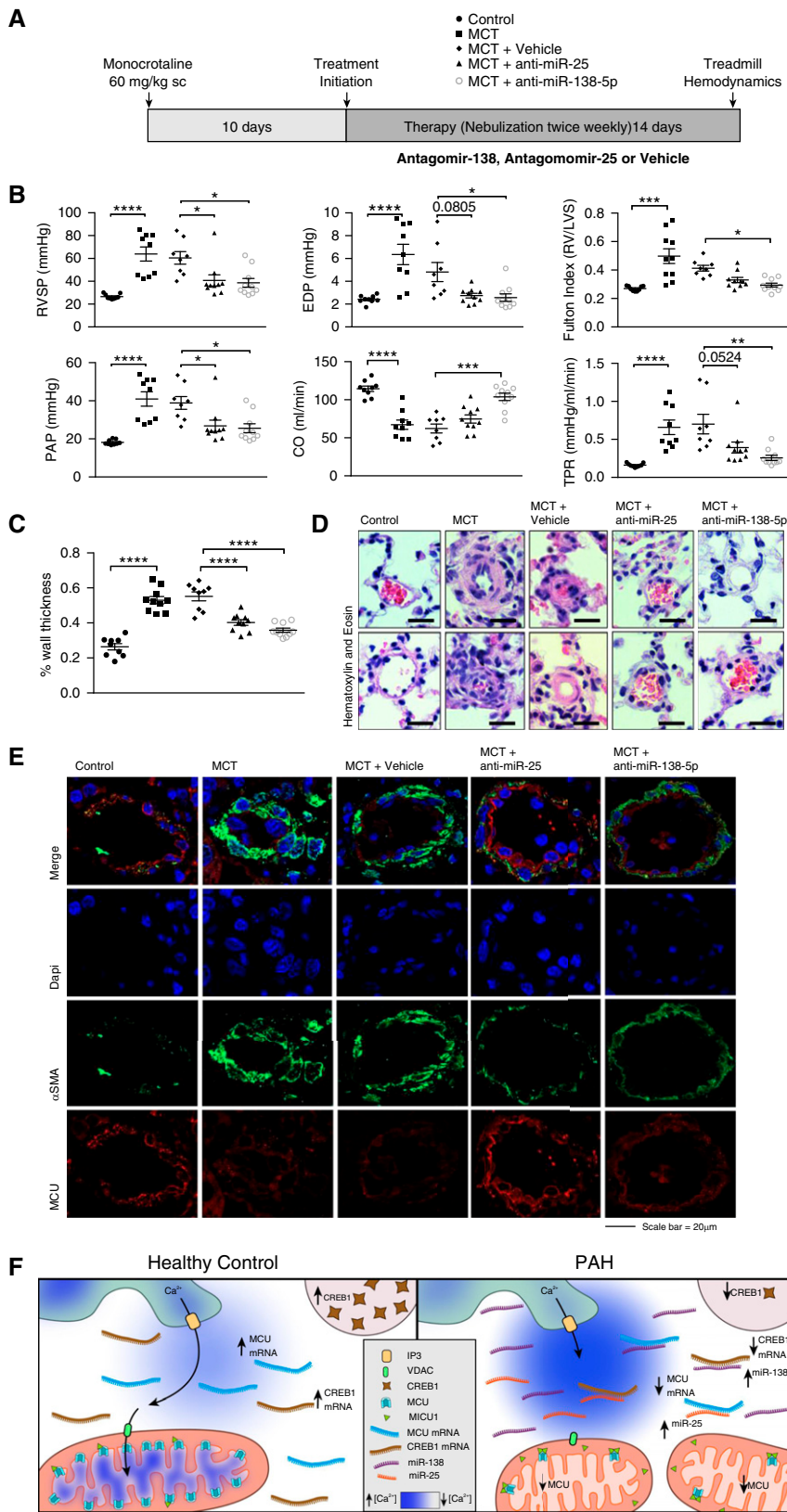
**Figure 6.** Anti-microRNA (miR) therapy regresses pulmonary arterial hypertension (PAH) *in vivo*. (*A*) Protocol for the administration of the anti-miRs in rats with established PAH. Ten days after injection of monocrotaline (MCT; 60 mg/kg subcutaneous; n = 10 rats/group) rats were anesthetized and

Finally, miR-138 is an important regulator of the DNA damage response, which has been implicated in the pathophysiology of PAH (50). Although the increase in miR-25 expression in PAH did not achieve statistical significance, the therapeutic response to anti–miR-25 confirms that it contributes to decreased MCU expression and to the pathogenesis of PAH (Figures 5B and 6B). MCU regulation by miR-25 has previously been described in cancer cells (29), although the effects of manipulating miR-25 on cell metabolism and proliferation rates had not previously been assessed.

In addition to post-transcriptional down-regulation of MCU, miR-25 and miR-138 reduce CREB1 activation in PAH (Figures 5E–5G). Prior studies reported a PDGF-initiated, PI3K/Akt-mediated CREB1 down-regulation in PASMCs from animals with hypoxic pulmonary hypertension, noting it increased PASMC migration and proliferation (51). We found that si-CREB1 reduces MCU expression in normal PASMCs (Figure 5E). However, using *in silico* technique we identified several sites in CREB1's 3′-UTR that are predicted to bind miR-138 and miR-25. Because CREB1 expression increases in response to both antagomirs this suggests the miRs are upstream of CREB1. Thus, in PAH MCU down-regulation occurs directly as a result of inhibition of MCU expression by the miRs, and indirectly by miR-induced CREB1 down-regulation.

The therapeutic potential of restoring MCU expression was tested directly (by MCU transfection in PASMCs) (Figures 2–4) and indirectly (miR-25 and miR-138 anti-miRs) (Figures 5B and 5C). Restoring MCU expression in PASMCs reduces mitochondrial fission (Figure 2), restores glucose oxidation, reverses the Warburg effect (Figure 3), and decreases the pathologic rates of cell motility and migration (52) and proliferation (4, 11) that characterize PAH (Figure 4). Although we show that the anti-miRs restore MCU expression in human PAH PASMCs (Figure 5C), the more rigorous test of therapeutic relevance was conducted *in vivo*. We demonstrated that nebulized antagomirs targeting miR-25 and miR-138 completely regressed MCT-induced PAH (Figure 6B; *see* Figure E9).

In our study, loss of MCU function is pathologic and therapeutic benefit is gained by restoring MCU expression;

however, disease context does matter. For example, mice with a homozygous deletion of MCU have normal cardiac function at rest and in response to increased afterload or isoproterenol (53). In conditions where intramitochondrial calcium is severely elevated, such as heart failure (54), subarachnoid hemorrhage (55), and ischemia reperfusion injury (30), inhibition of MCU may prevent mitochondrial further calcium overload and preserve organ function. For example, in cardiomyocytes, oxidative stress increases miR-25, which binds the 3′-UTR of MCU, down-regulating its expression and exerting a protective effect by decreasing excessive $H_2O_2$-induced increases in $[Ca^{2+}]_{mito}$

(30). These examples occur in a very different context than PAH, where MCU is down-regulated and intramitochondrial calcium concentrations are pathologically reduced.

The miR-MCU pathway is likely downstream from triggers of PAH that may be genetic (mutations of bone morphogenetic protein receptor 2), epigenetic (gene silencing by CpG methylation), environmental (related to toxins and drugs that modify the serotonin signaling pathway, such as dexfenfluramine), or inflammatory. Nonetheless, impaired MCUC activity, due largely to reduced MCU expression, constitutes a unifying mechanism

for the overload in $[Ca^{2+}]_{cyto}$ and reduction in $[Ca^{2+}]_{mito}$ that alter mitochondrial dynamics and metabolism, respectively, and which thereby drive PAH's cancer-like phenotype. Restoration of MCUC function has a large therapeutic benefit, whether achieved by plasmid transfection of the MCU gene in PASMCs or by nebulized anti-miRs *in vivo* (schematic, Figure 6E). This suggests MCU and $[Ca^{2+}]_{mito}$ are important new targets for therapy of proliferative, apoptosis-resistant diseases, such as PAH and cancer. ■

## References

1. Archer SL, Weir EK, Wilkins MR. Basic science of pulmonary arterial hypertension for clinicians: new concepts and experimental therapies. *Circulation* 2010;121:2045–2066.
2. Thenappan T, Shah SJ, Rich S, Gomberg-Maitland M. A USA-based registry for pulmonary arterial hypertension: 1982-2006. *Eur Respir J* 2007;30:1103–1110.
3. Sutendra G, Michelakis ED. The metabolic basis of pulmonary arterial hypertension. *Cell Metab* 2014;19:558–573.
4. Marsboom G, Toth PT, Ryan JJ, Hong Z, Wu X, Fang YH, Thenappan T, Piao L, Zhang HJ, Pogoriler J, et al. Dynamin-related protein 1-mediated mitochondrial mitotic fission permits hyperproliferation of vascular smooth muscle cells and offers a novel therapeutic target in pulmonary hypertension. *Circ Res* 2012;110:1484–1497.
5. Rehman J, Zhang HJ, Toth PT, Zhang Y, Marsboom G, Hong Z, Salgia R, Husain AN, Wietholt C, Archer SL. Inhibition of mitochondrial fission prevents cell cycle progression in lung cancer. *FASEB J* 2012;26:2175–2186.
6. Archer SL, Gomberg-Maitland M, Maitland ML, Rich S, Garcia JG, Weir EK. Mitochondrial metabolism, redox signaling, and fusion: a mitochondria-ROS-HIF-1alpha-Kv1.5 O2-sensing pathway at the intersection of pulmonary hypertension and cancer. *Am J Physiol Heart Circ Physiol* 2008;294:H570–H578.
7. Archer SL, Marsboom G, Kim GH, Zhang HJ, Toth PT, Svensson EC, Dyck JR, Gomberg-Maitland M, Thébaud B, Husain AN, et al. Epigenetic attenuation of mitochondrial superoxide dismutase 2 in

pulmonary arterial hypertension: a basis for excessive cell proliferation and a new therapeutic target. *Circulation* 2010;121:2661–2671.
8. Marsboom G, Wietholt C, Haney CR, Toth PT, Ryan JJ, Morrow E, Thenappan T, Bache-Wiig P, Piao L, Paul J, et al. Lung ¹⁸F-fluorodeoxyglucose positron emission tomography for diagnosis and monitoring of pulmonary arterial hypertension. *Am J Respir Crit Care Med* 2012;185:670–679.
9. Xu W, Erzurum SC. Endothelial cell energy metabolism, proliferation, and apoptosis in pulmonary hypertension. *Compr Physiol* 2011;1: 357–372.
10. Warburg O. On the origin of cancer cells. *Science* 1956;123: 309–314.
11. Ryan JJ, Marsboom G, Fang YH, Toth PT, Morrow E, Luo N, Piao L, Hong Z, Ericson K, Zhang HJ, et al. PGC1α-mediated mitofusin-2 deficiency in female rats and humans with pulmonary arterial hypertension. *Am J Respir Crit Care Med* 2013;187: 865–878.
12. Yuan JX, Aldinger AM, Juhaszova M, Wang J, Conte JV Jr, Gaine SP, Orens JB, Rubin LJ. Dysfunctional voltage-gated K+ channels in pulmonary artery smooth muscle cells of patients with primary pulmonary hypertension. *Circulation* 1998;98: 1400–1406.
13. Pozeg ZI, Michelakis ED, McMurtry MS, Thébaud B, Wu XC, Dyck JR, Hashimoto K, Wang S, Moudgil R, Harry G, et al. In vivo gene transfer of the O2-sensitive potassium channel Kv1.5 reduces pulmonary

**Figure 6.** (Continued). nebulized biweekly for 2 weeks with either negative control (5 nmol in 50 μl, mirVana miRNA inhibitor negative control#1, Ambion), anti–miR-25, or anti–miR-138 (5 nmol in 50 μl, mirVana miRNA inhibitor, Ambion). (B) Compared with control rats (n = 9), MCT caused severe PAH with elevations of total pulmonary vascular resistance (TPR) and right ventricular (RV) hypertrophy, evident as an increase in Fulton index, and RV failure, evident as an increase in end diastolic pressure (EDP). Anti–miR-138 was more effective than anti–miR-25 in increasing cardiac output (CO; *$P < 0.05$; **$P < 0.01$; ***$P < 0.001$; ****$P < 0.0001$). PAP = pulmonary arterial pressure; RVSP = right ventricle systolic pressure. (C) Summary data and (D) representative images demonstrating that the regression of PAH was accompanied by a reduction in the medial thickness of small pulmonary arteries (****$P < 0.0001$). Scale bar = 25 μm. (E) Representative immunofluorescence images of mitochondrial calcium uniporter (MCU) expression (red) in pulmonary arterioles (α-smooth muscle actin [αSMA], green) from MCT challenged rats, with and without treatment with nebulized anti–miR-25 or anti–miR-138. Nuclei are stained in blue. (F) Schematic illustrating the proposed model in which increases in miR-138, reinforced by increases in other miRs including miR-25, suppress both cAMP response element–binding protein 1 (CREB1) and the MCU itself. miR-138 directly inhibits expression of MCU and reinforces this effect indirectly by down-regulating CREB1. The loss of MCU expression, exacerbated by increased expression of mitochondrial calcium uptake protein 1 (MICU1), reduces the function of the MCU complex. This simultaneously overloads cytosolic calcium while depriving the mitochondria of the calcium. The former triggers pulmonary artery smooth muscle cell migration and proliferation (and vasoconstriction), whereas the latter affects the mitochondrion, inhibiting pyruvate dehydrogenase and promoting a shift to uncoupled glycolysis (the Warburg phenomenon), further driving cell proliferation and apoptosis resistance. Changes in intracellular calcium homeostasis also promote mitochondrial fission by activating Drp1, a known driver of cell proliferation (4). There are several major pathways for calcium extrusion from the matrix that were not studied, notably NCLX (recently identified Na⁺–Ca²⁺ exchanger [20]) and the H⁺–Ca²⁺ exchanger (21). It is possible that changes in efflux mechanisms might also occur in PAH. DAPI = 4′,6-diamidino-2-phenylindole [DAPI]; Drp1 = dynamin related protein 1; IP3 = inositol 1,4,5-trisphosphate receptor; LVS = left ventricle + septum; VDAC = voltage-dependent anion channel.

hypertension and restores hypoxic pulmonary vasoconstriction in chronically hypoxic rats. *Circulation* 2003;107:2037–2044.

14. Yu Y, Keller SH, Remillard CV, Safrina O, Nicholson A, Zhang SL, Jiang W, Vangala N, Landsberg JW, Wang JY, *et al*. A functional single-nucleotide polymorphism in the TRPC6 gene promoter associated with idiopathic pulmonary arterial hypertension. *Circulation* 2009; 119:2313–2322.

15. Pan X, Liu J, Nguyen T, Liu C, Sun J, Teng Y, Fergusson MM, Rovira II, Allen M, Springer DA, *et al*. The physiological role of mitochondrial calcium revealed by mice lacking the mitochondrial calcium uniporter. *Nat Cell Biol* 2013;15:1464–1472.

16. Denton RM, McCormack JG, Edgell NJ. Role of calcium ions in the regulation of intramitochondrial metabolism. Effects of Na+, Mg2+ and ruthenium red on the Ca2+-stimulated oxidation of oxoglutarate and on pyruvate dehydrogenase activity in intact rat heart mitochondria. *Biochem J* 1980;190:107–117.

17. McCormack JG, Denton RM. The role of intramitochondrial Ca2+ in the regulation of oxidative phosphorylation in mammalian tissues. *Biochem Soc Trans* 1993;21:793–799.

18. De Stefani D, Raffaello A, Teardo E, Szabò I, Rizzuto R. A forty-kilodalton protein of the inner membrane is the mitochondrial calcium uniporter. *Nature* 2011;476:336–340.

19. Raffaello A, De Stefani D, Sabbadin D, Teardo E, Merli G, Picard A, Checchetto V, Moro S, Szabò I, Rizzuto R. The mitochondrial calcium uniporter is a multimer that can include a dominant-negative pore-forming subunit. *EMBO J* 2013;32:2362–2376.

20. Palty R, Silverman WF, Hershfinkel M, Caporale T, Sensi SL, Parnis J, Nolte C, Fishman D, Shoshan-Barmatz V, Herrmann S, *et al*. NCLX is an essential component of mitochondrial Na+/Ca2+ exchange. *Proc Natl Acad Sci USA* 2010;107:436–441.

21. Takeuchi A, Kim B, Matsuoka S. The destiny of Ca(2+) released by mitochondria. *J Physiol Sci* 2015;65:11–24.

22. Kirichok Y, Krapivinsky G, Clapham DE. The mitochondrial calcium uniporter is a highly selective ion channel. *Nature* 2004;427: 360–364.

23. Samanta K, Douglas S, Parekh AB. Mitochondrial calcium uniporter MCU supports cytoplasmic Ca2+ oscillations, store-operated Ca2+ entry and Ca2+-dependent gene expression in response to receptor stimulation. *PLoS One* 2014;9:e101188.

24. Perocchi F, Gohil VM, Girgis HS, Bao XR, McCombs JE, Palmer AE, Mootha VK. MICU1 encodes a mitochondrial EF hand protein required for Ca(2+) uptake. *Nature* 2010;467:291–296.

25. Baughman JM, Perocchi F, Girgis HS, Plovanich M, Belcher-Timme CA, Sancak Y, Bao XR, Strittmatter L, Goldberger O, Bogorad RL, *et al*. Integrative genomics identifies MCU as an essential component of the mitochondrial calcium uniporter. *Nature* 2011; 476:341–345.

26. Kamer KJ, Mootha VK. The molecular era of the mitochondrial calcium uniporter. *Nat Rev Mol Cell Biol* 2015;16:545–553.

27. Pacher P, Hajnóczky G. Propagation of the apoptotic signal by mitochondrial waves. *EMBO J* 2001;20:4107–4121.

28. Shanmughapriya S, Rajan S, Hoffman NE, Zhang X, Guo S, Kolesar JE, Hines KJ, Ragheb J, Jog NR, Caricchio R, *et al*. Ca2+ signals regulate mitochondrial metabolism by stimulating CREB-mediated expression of the mitochondrial Ca2+ uniporter gene MCU. *Sci Signal* 2015;8:ra23.

29. Marchi S, Lupini L, Patergnani S, Rimessi A, Missiroli S, Bonora M, Bononi A, Corrà F, Giorgi C, De Marchi E, *et al*. Downregulation of the mitochondrial calcium uniporter by cancer-related miR-25. *Curr Biol* 2013;23:58–63.

30. Pan L, Huang BJ, Ma XE, Wang SY, Feng J, Lv F, Liu Y, Liu Y, Li CM, Liang DD, *et al*. MiR-25 protects cardiomyocytes against oxidative damage by targeting the mitochondrial calcium uniporter. *Int J Mol Sci* 2015;16:5420–5433.

31. Wang W, Kwon EJ, Tsai LH. MicroRNAs in learning, memory, and neurological diseases. *Learn Mem* 2012;19:359–368.

32. Parker D, Ferreri K, Nakajima T, LaMorte VJ, Evans R, Koerber SC, Hoeger C, Montminy MR. Phosphorylation of CREB at Ser-133 induces complex formation with CREB-binding protein via a direct mechanism. *Mol Cell Biol* 1996;16:694–703.

33. Dromparis P, Paulin R, Sutendra G, Qi AC, Bonnet S, Michelakis ED. Uncoupling protein 2 deficiency mimics the effects of hypoxia and endoplasmic reticulum stress on mitochondria and triggers pseudohypoxic pulmonary vascular remodeling and pulmonary hypertension. *Circ Res* 2013;113:126–136.

34. Archer SL. Mitochondrial dynamics: mitochondrial fission and fusion in human diseases. *N Engl J Med* 2013;369: 2236–2251.

35. Han XJ, Lu YF, Li SA, Kaitsuka T, Sato Y, Tomizawa K, Nairn AC, Takei K, Matsui H, Matsushita M. CaM kinase I alpha-induced phosphorylation of Drp1 regulates mitochondrial morphology. *J Cell Biol* 2008;182:573–585.

36. Boucherat O, Potus F, Bonnet S. microRNA and pulmonary hypertension. *Adv Exp Med Biol* 2015;888:237–252.

37. Grant JS, White K, MacLean MR, Baker AH. MicroRNAs in pulmonary arterial remodeling. *Cell Mol Life Sci* 2013;70: 4479–4494.

38. Potus F, Malenfant S, Graydon C, Mainguy V, Tremblay È, Breuils-Bonnet S, Ribeiro F, Porlier A, Maltais F, Bonnet S, *et al*. Impaired angiogenesis and peripheral muscle microcirculation loss contribute to exercise intolerance in pulmonary arterial hypertension. *Am J Respir Crit Care Med* 2014;190:318–328.

39. Potus F, Ruffenach G, Dahou A, Thebault C, Breuils-Bonnet S, Tremblay È, Nadeau V, Paradis R, Graydon C, Wong R, *et al*. Downregulation of MicroRNA-126 contributes to the failing right ventricle in pulmonary arterial hypertension. *Circulation* 2015;132: 932–943.

40. Li S, Ran Y, Zhang D, Chen J, Li S, Zhu D. MicroRNA-138 plays a role in hypoxic pulmonary vascular remodelling by targeting Mst1. *Biochem J* 2013;452:281–291.

41. Bertero T, Cottrill K, Krauszman A, Lu Y, Annis S, Hale A, Bhat B, Waxman AB, Chau BN, Kuebler WM, *et al*. The microRNA-130/301 family controls vasoconstriction in pulmonary hypertension. *J Biol Chem* 2015;290:2069–2085.

42. Huber LC, Ulrich S, Leuenberger C, Gassmann M, Vogel J, von Blotzheim LG, Speich R, Kohler M, Brock M. Featured article: microRNA-125a in pulmonary hypertension: regulator of a proliferative phenotype of endothelial cells. *Exp Biol Med (Maywood)* 2015;240:1580–1589.

43. Parikh VN, Jin RC, Rabello S, Gulbahce N, White K, Hale A, Cottrill KA, Shaik RS, Waxman AB, Zhang YY, *et al*. MicroRNA-21 integrates pathogenic signaling to control pulmonary hypertension: results of a network bioinformatics approach. *Circulation* 2012;125: 1520–1532.

44. Caruso P, Dempsie Y, Stevens HC, McDonald RA, Long L, Lu R, White K, Mair KM, McClure JD, Southwood M, *et al*. A role for miR-145 in pulmonary arterial hypertension: evidence from mouse models and patient samples. *Circ Res* 2012;111:290–300.

45. Li SS, Ran YJ, Zhang DD, Li SZ, Zhu D. MicroRNA-190 regulates hypoxic pulmonary vasoconstriction by targeting a voltage-gated K+ channel in arterial smooth muscle cells. *J Cell Biochem* 2014;115: 1196–1205.

46. Brock M, Trenkmann M, Gay RE, Michel BA, Gay S, Fischler M, Ulrich S, Speich R, Huber LC. Interleukin-6 modulates the expression of the bone morphogenic protein receptor type II through a novel STAT3-microRNA cluster 17/92 pathway. *Circ Res* 2009;104: 1184–1191.

47. Courboulin A, Paulin R, Giguère NJ, Saksouk N, Perreault T, Meloche J, Paquet ER, Biardel S, Provencher S, Côté J, *et al*. Role for miR-204 in human pulmonary arterial hypertension. *J Exp Med* 2011;208: 535–548.

48. Patergnani S, Giorgi C, Maniero S, Missiroli S, Maniscalco P, Bononi I, Martini F, Cavallesco G, Tognon M, Pinton P. The endoplasmic reticulum mitochondrial calcium cross talk is downregulated in malignant pleural mesothelioma cells and plays a critical role in apoptosis inhibition. *Oncotarget* 2015;6: 23427–23444.

49. Sen A, Ren S, Lerchenmüller C, Sun J, Weiss N, Most P, Peppel K. MicroRNA-138 regulates hypoxia-induced endothelial cell dysfunction by targeting S100A1. *PLoS One* 2013;8: e78684.

50. Meloche J, Pflieger A, Vaillancourt M, Paulin R, Potus F, Zervopoulos S, Graydon C, Courboulin A, Breuils-Bonnet S, Tremblay E, et al. Role for DNA damage signaling in pulmonary arterial hypertension. *Circulation* 2014;129:786–797.

51. Klemm DJ, Watson PA, Frid MG, Dempsey EC, Schaack J, Colton LA, Nesterova A, Stenmark KR, Reusch JE. cAMP response element-binding protein content is a molecular determinant of smooth muscle cell proliferation and migration. *J Biol Chem* 2001;276: 46132–46141.

52. Paulin R, Meloche J, Courboulin A, Lambert C, Haromy A, Courchesne A, Bonnet P, Provencher S, Michelakis ED, Bonnet S. Targeting cell motility in pulmonary arterial hypertension. *Eur Respir J* 2014;43:531–544.

53. Holmström KM, Pan X, Liu JC, Menazza S, Liu J, Nguyen TT, Pan H, Parks RJ, Anderson S, Noguchi A, et al. Assessment of cardiac function in mice lacking the mitochondrial calcium uniporter. *J Mol Cell Cardiol* 2015;85:178–182.

54. Santulli G, Xie W, Reiken SR, Marks AR. Mitochondrial calcium overload is a key determinant in heart failure. *Proc Natl Acad Sci USA* 2015;112:11389–11394.

55. Yan H, Zhang D, Hao S, Li K, Hang CH. Role of mitochondrial calcium uniporter in early brain injury after experimental subarachnoid hemorrhage. *Mol Neurobiol* 2015;52:1637–1647.

56. Palmer AE, Tsien RY. Measuring calcium signaling using genetically targetable fluorescent indicators. *Nat Protoc* 2006;1:1057–1065.